

Hydrofoil Cavitation Under Strong Thermodynamic Effect

Jonas P. R. Gustavsson
e-mail: jgu@ufl.edu

Kyle C. Denning

Corin Segal

Department of Mechanical and Aerospace
Engineering,
University of Florida,
P.O. Box 116250,
Gainesville, FL 32611

Cavitation was studied for a NACA0015 hydrofoil using a material that simulates cryogenic behavior. Several angles of attack and flow speeds up to 8.6 m/s were tested. The material used, 2-trifluoromethyl-1,1,1,2,4,4,5,5,5-nonafluoro-3-pentanone, hereafter referred to as fluoroketone, exhibits a strong thermodynamic effect even under ambient conditions. Static pressures were measured at seven chordwise locations along the centerline of the hydrofoil suction side and on the test section wall immediately upstream of the hydrofoil. Frequency analysis of the test section static pressure showed that the amplitude of the oscillations increased as the tunnel speed increased. A gradual transition corresponding to the Type II-I sheet cavitation transition observed in water was found to occur near $\sigma/2\alpha = 5$ with Strouhal numbers based on chord dropping from 0.5 to 0.1 as the cavitation number was reduced. Flash-exposure high-speed imaging showed the cavity covering a larger portion of the chord for a given cavitation number than in cold water. The bubbles appeared significantly smaller in the current study and the pressure data showed increasing rather than constant static pressure in the downstream direction in the cavitating region, in line with observations made in literature for other geometries with fluids exhibiting strong thermodynamic effect.

[DOI: 10.1115/1.2953297]

Introduction

Cavitation in cryogenic turbopumps, primarily in liquid-fuel rocket engine applications, is a long-standing but difficult phenomenon to study due to the combination of highly flammable liquids and extremely low temperatures involved. At the same time, the thermodynamic effect, which causes a localized drop in liquid temperature near the vapor bubble formation due to vaporization, is significantly stronger in cryogenics than in water at moderate temperature and pressure. Water has been by far the most common medium for cavitation investigations. In a study by Ruggeri and Gelder [1], comparing cavitation of water and liquid nitrogen in a venturi, it was found that the temperature drop was an order of magnitude larger and the cavitation was frothier for liquid nitrogen when compared to water. Tani and Nagashima [2] carried out similar tests in a 2D Laval nozzle and found that the static pressure in the cavitating region remained constant and equal to the vapor pressure when water was used. When the test was repeated with liquid nitrogen, pressures below the nitrogen saturation vapor pressure—based on inlet temperature—were found in the cavitating region accompanied by a slight increase in pressure toward the nozzle exit. To quantify the thermodynamic effect, a nominal temperature depression ΔT^* and the ratio between the actual temperature drop and ΔT^* , known as the B -factor, have been introduced as follows [3]:

$$\Delta T^* = \frac{\Delta H_{\text{vap}} \rho_v}{C_{p,l} \rho_l} \quad (1)$$

$$B = \frac{\Delta T}{\Delta T^*} \quad (2)$$

where ΔH_{vap} is the latent heat of vaporization, $C_{p,l}$ is the liquid heat capacity, ρ_v is the vapor density, and ρ_l is the liquid density. Numerous correlations have been suggested to relate the B -factor to flow geometry and fluid properties, e.g., by Franc et al. [3], Billet et al. [4], and Hord [5]. The large range of correlations

suggests that there is still a need to understand which are the dominant parameters. Therefore, extrapolation of the cavitation behavior from one fluid to another with considerably different characteristics, such as water versus cryogenics, is risky. In the present investigation, a perfluorinated ketone, $\text{CF}_3\text{CF}_2\text{C}(\text{O})\text{CF}(\text{CF}_3)_2$, has been used to simulate the behavior of liquid hydrogen under the conditions present in a low-pressure turbopump rather than ambient water. Water has to be brought to very high temperature to attain a similar ΔT^* , as Table 1 indicates. At ambient conditions, ΔT^* is 20 times higher in fluoroketone than in water. This is due to the liquid/vapor density ratio, which is two orders of magnitude smaller for fluoroketone than for water under ambient conditions. Furthermore, the fluoroketone has low kinematic viscosity, $3.3 \times 10^{-7} \text{ m}^2/\text{s}$ at ambient conditions, facilitating high-Re testing at low speeds. Other parameters may also need to be considered, potentially using a B -factor model.

The present study allows the cavitation number, angle of attack, and geometry to be matched against water tests in literature, isolating the effect of ΔT^* to provide further insights in cavitation modeling. The cavitation number σ used here is defined as:

$$\sigma \equiv \frac{P_\infty - P_{\text{vap}}(T_\infty)}{\frac{1}{2} \rho_{l,\infty} U_\infty^2} \quad (3)$$

Here, P_∞ is the freestream static pressure, P_{vap} is the vapor pressure, T_∞ is the freestream temperature, $\rho_{l,\infty}$ is the freestream liquid density, and U_∞ is the freestream flow speed.

In the present study, pressure fluctuations and cavitation morphology for sheet and cloud cavitation in fluoroketone at varying angles of attack and cavitation numbers were investigated at speeds up to 8.6 m/s. Several studies with similar goals have been carried out in water, e.g., by Coutier-Delgosha et al. [6] and Cervone et al. [7]. Coutier-Delgosha et al. [6] studied the morphology of cavitation in water on the flat suction side of a hydrofoil with a convex pressure side using an embedded endoscope. This study concluded that the common assumption of spherical bubbles and symmetry in structure between a mostly liquid flow with a few bubbles and a mostly vapor-filled fluid with a few droplets are both invalid in the studied case. Rather, the cavitating region was filled with deformed, interacting bubbles of varying sizes at high liquid volume fractions, and there were no isolated liquid droplets

Contributed by the Fluids Engineering Division of ASME for publication in the JOURNAL OF FLUIDS ENGINEERING. Manuscript received August 29, 2007; final manuscript received May 8, 2008; published online August 12, 2008. Assoc. Editor: Steven Ceccio.

Table 1 Comparison of properties near ambient conditions for fluoroketone and water to liquid hydrogen at cryogenic pump inlet conditions. $Re^{0.2}Pr^{0.7}$ is a B -factor scaling suggested by Franc et al. [3]. The Reynolds number is based on the present study geometry with $c=51$ mm, $U_\infty=8.6$ m/s.

	Fluoroketone 25 °C	Fluoroketone 49 °C	Hydrogen 22.8 K	Water 25 °C	Water 75 °C	Water 110 °C
p_v (MPa)	0.04	0.10	0.20	0.003	0.039	0.152
p_c (MPa)	1.87	1.87	1.3	22.06	22.06	22.06
T_c (K)	442	442	33	647	647	647
$\rho_l/\rho_{v,sat}$	310	119	27	42842	4031	1104
ΔT^* (K)	0.3	0.7	1.4	0.014	0.137	0.478
Pr	8.2	9.3	1.2	6.1	2.4	1.6
Re	1.3E+06	1.5E+06	2.7E+06	4.9E+05	1.1E+06	1.6E+06
$Re^{0.2}Pr^{0.7}$	73	82	22	49	30	24

in the vapor region under low liquid volume fraction conditions. The maximum void fraction increased rapidly from 0.55 to 0.80 as the cavitation number decreased from 0.7 to 0.6, which also marked the transition to supercavitation on that particular hydrofoil. The dominant measured fluctuation frequency was normalized giving the Strouhal numbers based on cavity and chord length, respectively.

$$St_{L_{cav}} = \frac{L_{cav}f}{U_\infty} \quad (4)$$

$$St_c = \frac{cf}{U_\infty} \quad (5)$$

where L_{cav} is the cavity streamwise length, c is the chord length, and f is the observed dominant frequency of oscillations. Strouhal numbers based on cavity length of about 0.25 were seen for short, $L_{cav}/c < 0.75$, conditions and $St_{L_{cav}} = 0.12$ for long cavities, $L_{cav}/c > 0.75$. Cervone et al. [7], who used a NACA0015 hydrofoil in water at varying temperature and angles of attack, α , noted a strengthening of the visible cavitation with increasing temperature when α and σ were kept constant. The surface pressure, however, still showed that increasing temperature had the effect of shortening the cavitation plateau and increasing the $-(C_{Pmin})$; in fact, at $\alpha=5$ deg, $\sigma=1.5$, pressures similar to those measured under cavitation-free conditions were measured. A fundamental fluctuation Strouhal number was found at $St_c=0.17$ over a wide range of cavitation numbers, $1.3 < \sigma < 2.1$ at $\alpha=8$ deg and $25 < T_\infty < 70$ °C. A weaker higher-frequency peak, potentially a higher harmonic, was also observed by Cervone et al. [7] for $1.4 < \sigma < 2.1$ near $St_c=0.32$. A somewhat different behavior was observed on a NACA0015 hydrofoil at $\alpha=7$ deg in water by Kjeldsen et al. [9]. For $0.75 < \sigma < 1$, $St_c=0.15$ Mode I oscillations dominated, while for $1 < \sigma < 1.3$, Mode II oscillations at $St_{L_{cav}}=0.3$ became more prominent.

Experimental Setup

The hydrofoil used in the present study had a NACA0015 profile, a 102 mm span, and a 51 mm chord. A closed-loop facility was filled with the perfluorinated ketone described above. The facility is driven by a 25 hp pump controlled by a Danfoss VLT 5022 controller that allows the speed of the pump to be controllably varied. A sketch of the facility is shown in Fig. 1. To reduce the tendency of vapor bubbles to circulate and accumulate, as noticed frequently in closed-loop facilities, three fine-meshed screens in series, the finest with 0.074 mm openings, were placed in the stagnation chamber. The facility has a test section cross section of 102×102 mm² and is capable of providing flow speeds of up to 10 m/s. The tunnel is connected to an argon-based purge and vacuum systems to reduce the levels of dissolved gases in the fluid, primarily oxygen, which would affect incipient cavitation.

Prior to testing, vacuum down to 50 kPa is applied followed by repressurization with argon. This process is repeated for several hours to degas the fluoroketone. The hydrofoil was fitted with seven 1 mm diameter pressure taps along the centerline chord at $x/c=0.000, 0.056, 0.113, 0.168, 0.212, 0.317,$ and 0.883 , with x being a chordwise coordinate measured from the leading edge. One transducer measured the static pressure at the test section ceiling 25 mm upstream of the hydrofoil leading edge. The taps were connected to 30 psi (absolute) (0.2 MPa) Omega PX303 transducers using 0.2 m long nylon tubings with 1.5 mm inside diameter (i.d). A flush-mounted PCB1502 transducer is placed on the test section wall to ensure fast response. In addition, the tunnel is instrumented with 100 psi (absolute) (0.7 MPa) PX303 transducers connected to the stagnation chamber and the downstream collection box, as well as with RTDs on the stagnation chamber and the pump inlet to monitor fluid temperature, maintained ambient in this study. The 200 mm diameter pump outlet is equipped with a Prandtl probe connected to an Omega PX138 1 psi (differential) (7 kPa) transducer to monitor flow speed. All sensor outputs were recorded at 1 kHz during the tests.

In addition to pressure and temperature measurements, high-speed photography was used to capture the structure and temporal behavior of the cavitation at high speeds. Using a Cooke pco.1200 s camera synchronized with two flash units, a series of 16 sequential images was taken at a frame rate of 1270 fps along the span of the hydrofoil with illumination provided from the top. The flashes were spaced by 5.3 ms and covered a 10 mm wide slice near the centerline of the hydrofoil. Images were acquired with 50 μ s exposure time, and corrected for background illumination and variation of light intensity between images caused by the flash light decay over time.

Pressure data at steady conditions, typically the last 10–20 s prior to the next change in tunnel speed, were averaged to obtain hydrofoil C_p curves and frequency spectra. This involved fitting a

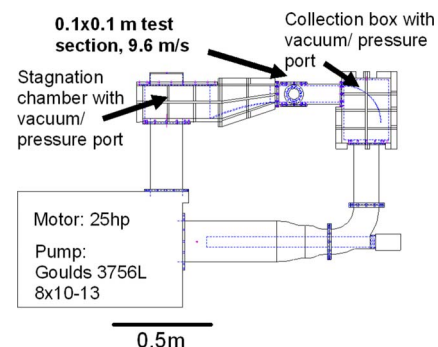


Fig. 1 Water tunnel test facility

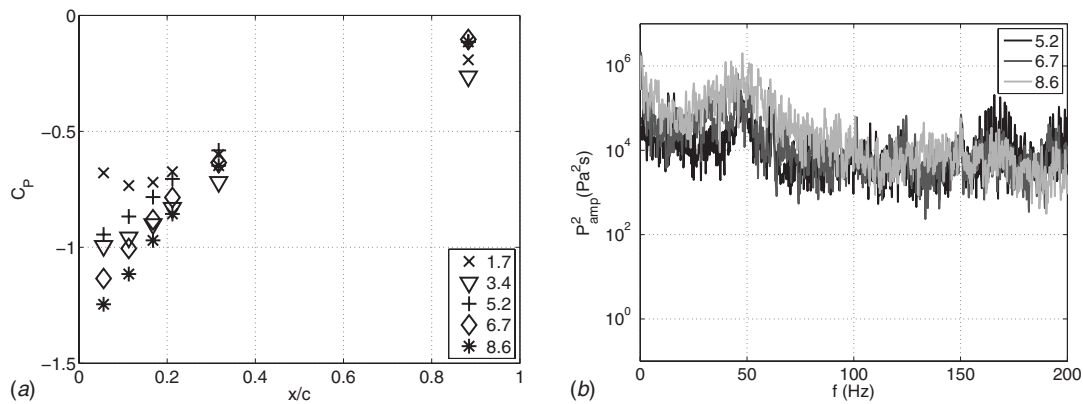


Fig. 2 Suction side pressure coefficient at different freestream speeds (left) and energy spectra at the test section static tap (right) at various freestream flow speeds in m/s; $\alpha=4$ deg, $\sigma=2.92$ at 5.2 m/s, $\sigma=2.14$ at 6.7 m/s, and $\sigma=1.67$ at 8.6 m/s

linear base line to the selected data, eliminating slow pressure drift seen in the tests, application of a Hanning filter followed by Fourier transformation of the data. The spectra were then low-pass filtered with a 0.1 Hz wide Gaussian filter for clarity before being plotted.

Uncertainties

The Omega PX303 transducer readings have a total uncertainty of 1.2% FS, corresponding to 2.4 kPa. The test section static pres-

sure transducer PCB1502 used in Figs. 2 and 3 has a total uncertainty of 0.7%, corresponding to 1.4 kPa. The tubings used in Fig. 4 have been found in pressure response tests to give a time constant of 20 ms, i.e., $1/e$ damping of oscillations at 50 Hz as well as a pumping pressure shift of 14 kPa during the test. The direct-connect PCB transducer exhibited significantly better response with negligible damping over the frequency region studied as well as negligible pumping effect. Due to the large range of dynamic pressures used in the C_p calculations, from 2.3 kPa at

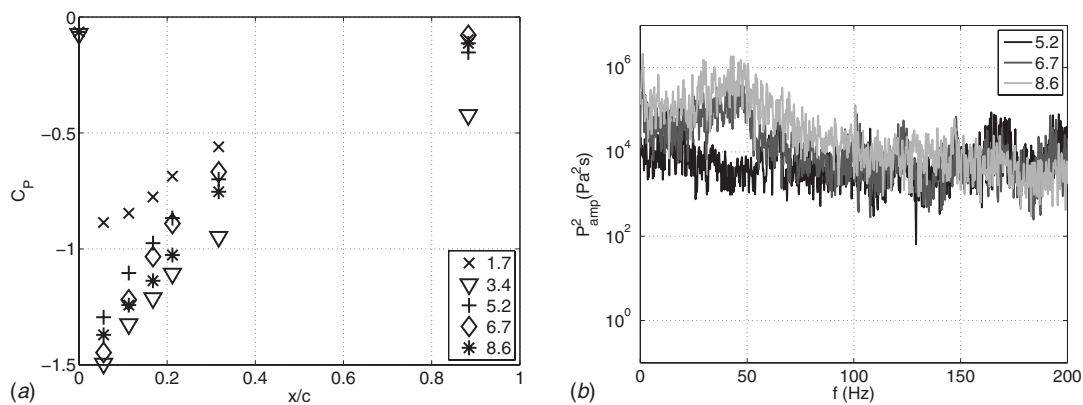


Fig. 3 Suction side pressure coefficient at different freestream speeds (left) and energy spectra at the test section static tap (right) at various freestream flow speeds in m/s; $\alpha=6.6$ deg, $\sigma=2.80$ at 5.2 m/s, $\sigma=2.00$ at 6.7 m/s, and $\sigma=1.54$ at 8.6 m/s

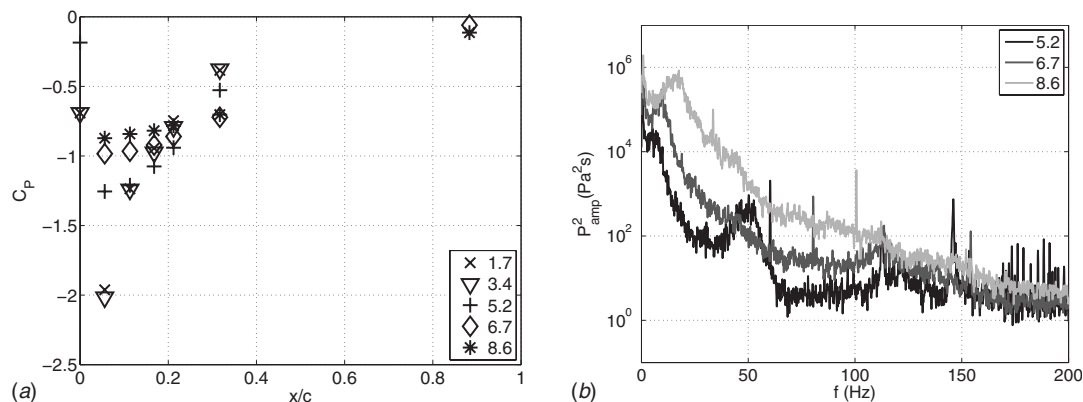


Fig. 4 Suction side pressure coefficient at different freestream speeds (left) and energy spectra at the test section static tap (right) at various freestream flow speeds in m/s; $\alpha=8$ deg, $\sigma=1.53$ at 5.2 m/s, $\sigma=1.21$ at 6.7 m/s, and $\sigma=1.06$ at 8.6 m/s

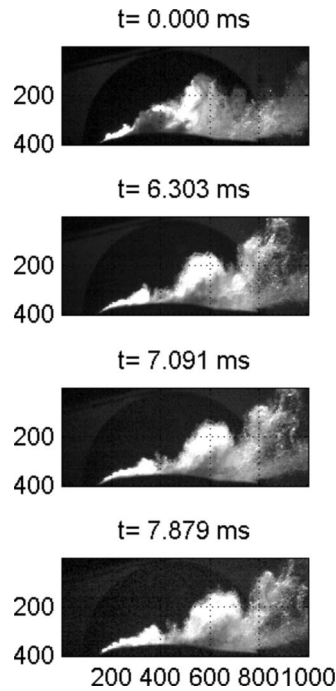


Fig. 5 Vapor formation on suction side of NACA0015 hydrofoil captured at 1270 fps at 5.2 m/s, 8 deg angle of attack at $\sigma = 1.53$. Flow from left to right, leading edge at horizontal pixel 146, trailing edge at 773, scale: 81 $\mu\text{m}/\text{pixel}$.

1.7 m/s to 59 kPa at 8.6 m/s, the uncertainty in C_p decreases from 1.2 to 0.05 as the speed increases from 1.7 m/s to 8.6 m/s.

Results

Using the system described above, pressure data were acquired at three different angles of attack and at various tunnel speeds. The time-averaged pressure coefficients and energy spectra at the test section static port are shown in Figs. 2–4. Spectra are only shown for the three highest tunnel speeds for clarity. For the cases shown in Figs. 2 and 3, the spectra had the same $\sim 10^4 \text{ Pa}^2 \text{ s}$ base line as the higher-speed tests, but with a weaker or missing broad 50 Hz peak. In the $\alpha = 8$ deg case, the oscillations were at the $1 \text{ Pa}^2 \text{ s}$ base line at 50 Hz and below $10^4 \text{ Pa}^2 \text{ s}$ at 10 Hz.

At the two smaller angles of attack, displayed in Figs. 2 and 3, the suction peak is not flattened as the speed is increased, and no significant oscillations are seen in the spectra. In contrast, at the $\alpha = 8$ deg case, shown in Fig. 4, cavitation is indicated by the decrease in the suction peak as speed is increased and the development of peaks in the frequency spectra near 50 Hz at 5.2 m/s and at around 10 Hz primarily for the two higher speeds. Also shown in Fig. 4 are the spikes corresponding to the pump blade passing frequency, e.g., at 100 Hz at 8.6 m/s tunnel speed. Response tests suggested that these oscillations are dampened, an order of magnitude due to the tubing damping in Fig. 4, while the spectra in Figs. 2 and 3 were taken using the flush-mounted PCB transducer, offering improved frequency response.

The sequence of images shown in Fig. 5 illustrates how the region filled with small vapor bubbles exhibits large thickness fluctuations but generally grows in the downstream direction. Also seen is a periodicity of 7 ms, suggesting a frequency of 140 Hz, corresponding to a peak in the spectrum shown in Fig. 4.

Discussion

Similar to the results obtained by Tani and Nagashima [2] in a 2D nozzle using liquid hydrogen and predicted by CFD modeling using the barotropic model of Rapposelli and d'Agostino [8] on a

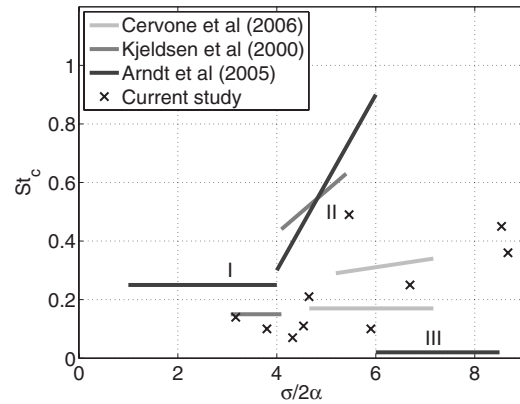


Fig. 6 Strouhal number of dominant frequency based on hydrofoil chord length plotted versus angle of attack-corrected cavitation number for several water studies. The three types of oscillatory behavior suggested by Arndt et al. [11] are indicated by Roman numerals. Conditions for tests where significant oscillations were seen in fluoroketone are indicated by x.

NACA 66-109 hydrofoil, the C_p curve during cavitation in Fig. 4 shows a slight increase rather than remaining absolutely flat following $-(C_{p\text{min}})$ as is seen in tests with negligible thermodynamic effect. While the pressure plateau shortening and increased $-(C_{p\text{min}})$ predicted by the Rapposelli and d'Agostino model [9] are also found in NACA0015 tests [7], the streamwise increase in pressure is not. In the present tests, the minimum pressure at the $x/c = 0.056$ tap appears to be about $0.2q$ higher than the freestream vapor pressure. It is possible that, given the spacing between the pressure taps, the suction peak possibly resides between the two upstream-most taps. The pressure increase downstream of the cavity is also gradual, unlike the shocklike rapid pressure rise predicted by the Rapposelli and d'Agostino model [8].

Comparing the present results to those obtained by Kjeldsen et al. [9] using a NACA0015 in ambient temperature degassed water general agreement in the occurrence of a Type I–II transition for $\sigma/2\alpha = 5$ rather than 4 is suggested by Fig. 4. Mode II oscillations observed for higher cavitation numbers appear to be increasingly indistinct as the cavitation number increases. At $\sigma = 1.53$ and $\alpha = 8$ deg, the broad peak is centered at $St_c = 0.49$, close to the 0.60 obtained from the Kjeldsen [9] correlation, but for other runs, the dominant frequency in this range is much lower. Several differences were noted. The difference in spectra between $\sigma = 2.80$ and $\sigma = 2.00$ at 6.6 deg, as shown in Fig. 3(b), suggests inception in the range $8.6 < \sigma/2\alpha < 12$, close to the inception criterion of $\sigma/2\alpha < 8.5$ based on data of Kjeldsen et al. [9]. In Fig. 3 range, no effect was seen on the C_p suction peak, but the local pressures remained above freestream vapor pressure. The general trend of St_c increasing with σ for Mode II oscillations seen by Kjeldsen et al. [9] was also observed in the present study but with significant scatter, as seen in Fig. 6. The increasing trend was noticed on a flat plate hydrofoil in tests by Sato et al. [10] where St_c increased from 0.3 up to 1.3 as the cavity length was decreased from $L_{\text{cav}}/c = 0.8$ to $L_{\text{cav}}/c = 0.15$. In that study, it was found that St_c could vary by a factor of 2 for the same L_{cav}/c depending on the test section inlet length, suggesting that this kind of oscillation may be facility dependent. This is also suggested by the data of Cervone et al. [7], which found St_c remaining close to 0.17 for a range of σ , and also observed what could be a second harmonic of this frequency, as shown in Fig. 6.

The appearance of the cavitation is also quite different in the present study with the cavitating region stretching across the entire hydrofoil chord even immediately after transition at 5.2 m/s, rather than covering less than 73% of the chord throughout the Type II regime, when $1.0 < \sigma < 1.3$ at 7 deg, as suggested by

Kjeldsen et al. [9]. In the high-speed photographs obtained by Wang et al. [12] in water on a Clark Y hydrofoil at 8 deg and $\sigma = 0.80$, the vapor phase was completely removed from the hydrofoil as a re-entrant jet washes it away from the surface starting at the trailing edge. In the present study, the vapor layer thickness fluctuates as much as a factor of 3 over time at a given chordwise position, but it was never completely absent, even at a moderate cavitation number of $\sigma = 1.53$ at $\alpha = 8$ deg. At this cavitation number, Wang et al. [12] found transition from incipient cavitation to attached small sheet cavitation. This further supports the conclusion that when matching σ , visually more extensive cavitation is present in fluoroketone than in water. This trend is also supported by the observations of Cervone et al. [7], who found that increasing water temperature while keeping α and σ constant generally expanded the visually cavitating region.

The cavitation observed in the present high-speed photographs in Fig. 5 exhibited a frothy appearance with a much finer structure than in water under ambient conditions, as noted for example, by Cervone et al. [7], who noted a trend toward smaller bubbles at higher water temperature and ΔT^* . It is also in line with the fine bubbles observed in liquid nitrogen by Ruggeri and Gelder [1].

Conclusions

Based on pressure measurements and high-speed photographs of cavitation in fluoroketone on a NACA0015 hydrofoil over a range of angles of attack and flow speeds, the following conclusions were drawn.

- The smaller bubbles and finer structures in cavitation observed in the present study compared to water tests, especially at ambient temperature, are attributed to a thermodynamic effect; the surface tension may also be responsible.
- The visual extent of cavitation is enlarged by increasing the thermodynamic effect while keeping the cavitation number constant.
- A large scatter in the frequency of Type II oscillations was

found between different studies, supporting the claim by Sato et al. [10] that these are facility-dependent oscillations.

- A gradual Type I-II transition was found near $\sigma/2\alpha = 5$, which is higher than observed in water.

Acknowledgment

This work has been supported by a NASA grant under the Constellation University Institute Program (CUIP). Ms. Claudia Meyer is the CUIP Manager. The authors would like to thank Dr. Dan Dorney from NASA MFSC for his continuous advice.

References

- [1] Ruggeri, R. S., and Gelder, T. F., 1964, "Cavitation and Effective Liquid Tension of Nitrogen in a Tunnel Venturi," NASA Report No. TN D-2088.
- [2] Tani, N., and Nagashima, T., 2003, "Cryogenic Cavitating Flow in 2D Laval Nozzle," *J. Therm. Sci.*, **12**(2), pp. 157–161.
- [3] Franc, J.-P., Rebattet, C., and Coulon, A., 2003, "An Experimental Investigation of Thermal Effects in a Cavitating Inducer," *Fifth International Symposium on Cavitation (Cav2003)*, Osaka, Japan.
- [4] Billet, M. L., Holl, J. W., and Weir, D. S., 1981, "Correlations of Thermodynamic Effects for Developed Cavitation," *ASME J. Fluids Eng.*, **103**(12), pp. 534–542.
- [5] Hord, J., 1973, "Cavitation in Liquid Cryogenics," NASA Report No. CR-2156.
- [6] Coutier-Delgosha, O., Devilliers, J.-F., Pichon, T., Vabre, A., Woo, R., and Legoupil, S., 2006, "Internal Structure and Dynamics of Sheet Cavitation," *Phys. Fluids*, **18**(1), p. 017103.
- [7] Cervone, A., Bramanti, C., Rapposelli, E., and d'Agostino, L., 2006, "Thermal Cavitation Experiments on a NACA 0015 Hydrofoil," *ASME J. Fluids Eng.*, **128**(2), pp. 326–331.
- [8] Rapposelli, E., and d'Agostino, L., 2003, "A Barotropic Cavitation Model With Thermodynamic Effects," *Fifth International Symposium on Cavitation (Cav2003)*, Osaka, Japan.
- [9] Kjeldsen, M., Arndt, R. E. A., and Effertz, M., 2000, "Spectral Characterization of Sheet/Cloud Cavitation," *ASME J. Fluids Eng.*, **122**(9), pp. 481–487.
- [10] Sato, K., Tanada, M., Monden, S., and Ysujimoto, Y., 2001, "Observations of Oscillating Cavitation of a Flat Plate Hydrofoil," *Fourth International Symposium on Cavitation (CAV2001)*, Pasadena, CA.
- [11] Arndt, R. E. A., Balas, G. J., and Wosnik, M., 2005, "Control of Cavitating Flows: A Perspective," *JSME Int. J., Ser. B*, **48**(2), pp. 334–341.
- [12] Wang, G., Senocak, I., Shyy, W., Ikohagi, T., and Cao, S., 2001, "Dynamics of Attached Turbulent Cavitating Flows," *Prog. Aerosp. Sci.*, **37**, pp. 551–581.